

**Nematic order by thermal disorder
in a three-dimensional lattice-spin model
with dipolar-like interactions**

Hassan Chamati¹ and Silvano Romano²

¹*Institute of Solid State Physics, Bulgarian Academy of Sciences,
72 Tzarigradsko Chaussée, 1784 Sofia (Bulgaria)*
chamati@bas.bg

²*Physics dept., the University, via A. Bassi 6, 27100 Pavia (Italy)*
silvano.romano@pv.infn.it

(Dated: May 28, 2022)

Abstract

At low temperatures, some lattice spin models with simple ferromagnetic or antiferromagnetic interactions (for example nearest-neighbour interaction being isotropic in spin space on a bipartite three-dimensional lattice) produce orientationally ordered phases exhibiting nematic (second-rank) order, in addition to the primary first-rank one; on the other hand, in the Literature, they have been rather seldom investigated in this respect. Here we study the thermodynamic properties of a three-dimensional model with dipolar-like interaction. Its ground state is found to exhibit full orientational order with respect to a suitably defined staggered magnetization (polarization), but no nematic second-rank order. Extensive Monte Carlo simulations, in conjunction with Finite-Size Scaling analysis have been used for characterizing its critical behaviour; on the other hand, it has been found that nematic order does indeed set in at low temperatures, via a mechanism of order by disorder.

PACS numbers: 05.50.+q, 64.60.-i, 75.10.Hk

I. INTRODUCTION

By now, multipole moments of specific, comparatively simple molecules, have been measured experimentally, or estimated by quantum mechanical calculations at various levels of approximation for some decades [1–3] (a recent example of method benchmarking can be found in Ref. [4]), and the corresponding interaction terms are important parts [3] of the relevant pair potentials, often used as starting points for further investigations, e.g. by simulation [5] (by definition, multipole moments are global single-centre quantities; actually, in force fields used for more complex molecules, e.g. in biomolecular simulations, electrostatic intermolecular interactions are usually represented in terms of point charges sitting on individual nuclei; usage of distributed point multipoles has also been proposed and advocated; e.g., the discussion in Refs. [3, 6]). On the other hand, there have been in the Literature also studies of further simplified, purely multipolar potential models, where particle centres of mass are associated with some regular lattice, and their interactions *only* involve multipolar terms of some order (say, dipole or quadrupole).

Notice, for example, that both electrostatic and magnetostatic dipolar interactions have the same mathematical structure (within numerical factors and usage of different units or symbols), which can thus be interpreted and used either way: the former interpretation is used in the study of molecular fluid or condensed phases (including mesogenic models), and the latter for dipolar contributions to magnetic lattice spin models, as well as in connection with ferrofluids [7]; in the following, we shall be using the magnetic language.

Let us also recall that, on the one hand, proper multipolar interactions are rather long-ranged (LR) and their treatment usually requires Ewald–Kornfeld or reaction–field approaches [5]; on the other hand, lattice interaction models defined by short-range interactions *with the same orientational dependence* as their LR counterparts are also known in the Literature.

Notice also that pair potential models used to study fluid or solid systems do also contain some additional term, such as hard sphere or Lennard–Jones in the simplest cases, ensuring short-range repulsion between the interacting particles. The above interaction models might produce low-temperature phases exhibiting orientational order; more precisely, various simulation studies show that, in three dimensions, dipolar hard spheres produce a ferroelectrically (ferromagnetically) ordered fluid phases (see Ref. [8] and others quoted therein), also exhibiting nematic order. Various pieces of evidence also suggest the existence of a low-temperature ordering transition for purely dipolar (or rather dipolar-like) lattice models; this result could be proven mathematically

for nearest-neighbour interactions of dipolar type on a simple-cubic lattice, in Ref. [9]; one of us had studied the model by simulation [10], and estimated its transitional behaviour. The existence of a low-temperature ordering transition for LR dipolar interactions on a simple-cubic lattice was later proven rigorously in Ref. [11].

In keeping with Ref. [10], we are considering a classical system consisting of n -component magnetic moments to be denoted by unit vectors $\{\mathbf{u}_j\}$, with Cartesian components $u_{j,\iota}$, associated with a d -dimensional lattice \mathbb{Z}^d (here $d = n = 3$), and interacting via a translationally invariant pair potential of the form

$$V_{ij} = \epsilon f(r) [-3(\mathbf{u}_i \cdot \hat{\mathbf{r}}_{ij})(\mathbf{u}_j \cdot \hat{\mathbf{r}}_{ij}) + \mathbf{u}_i \cdot \mathbf{u}_j], \quad (1)$$

with ϵ a positive quantity setting energy and temperature scales (i.e. energies will be expressed in units of ϵ , and temperatures defined by $T = k_B \mathcal{T}_K / \epsilon$, where \mathcal{T}_K denotes the temperature in degrees Kelvin), and

$$\mathbf{r}_{ij} = \mathbf{x}_i - \mathbf{x}_j, \quad r = |\mathbf{r}_{ij}|, \quad \hat{\mathbf{r}}_{ij} = \frac{\mathbf{r}_{ij}}{r}, \quad f(r) > 0;$$

here \mathbf{x}_j denotes the dimensionless lattice site coordinates, and the function $f(r)$ can describe algebraically decaying long-range interactions according to $f(r) = r^{-3}$, or be restricted to nearest neighbouring pairs (SR model, in which case $f(r) = 1$ for $r = 1$ and 0 otherwise), as in the case considered here.

In this paper we reinvestigate the transitional behavior resulting from the interaction potential (1). We start by defining the appropriate orientational quantities, such as the staggered magnetization, and their ground-state behaviour. In the ground state, we found evidence of orientational magnetic order and *absence* of the nematic one, as opposed to the behaviour of some lattice spin models with a fraction of sites randomly occupied by non-magnetic impurities and involving nearest-neighbour interaction, where both kinds of ordering were present [12–14]. Extensive Monte Carlo simulations for system sizes larger than those used in Ref. [10] showed evidence of nematic order by disorder in a low-temperature range.

The rest of our paper is organised as follows: in Section II we present our results for the ground state of interaction potential (1). The simulation methodology is discussed in Section III, and in Section IV simulation results and Finite-Size Scaling analysis are used to extract the critical behavior for the model under consideration. We conclude the paper with Section V where we summarize our results. In the Appendix we present a detailed derivation of analytical results needed in the paper.

II. THE GROUND STATE

For the sake of completeness we recall here some properties of the continuously degenerate ground state for the three-dimensional case ($d = 3$), following the corresponding section in the previous paper [10], where relevant results for the two-dimensional ($d = 2$), as well as for the fully long-ranged counterparts are also mentioned. Let lattice site coordinates be expressed as $\mathbf{x}_j = \mathbf{x}(h, k, l) = h\mathbf{e}_1 + k\mathbf{e}_2 + l\mathbf{e}_3$, $d = 3$, where \mathbf{e}_α denotes unit vectors along the lattice axes; here the subscript in h_j has been omitted for ease of notation; let also $\varrho_h = (-1)^h$, $\sigma_{hk} = \varrho_h \varrho_k$, $\tau_{hkl} = \varrho_h \varrho_k \varrho_l$.

The ground state possesses continuous degeneracy; its energy per particle is $E_0^* = -4$, and the manifold of its possible configurations is defined by

$$\mathbf{u}_j^0 = \mathbf{u}^0(h, k, l) = \sigma_{kl} N_1 \mathbf{e}_1 + \sigma_{hl} N_2 \mathbf{e}_2 + \sigma_{hk} N_3 \mathbf{e}_3, \quad (2)$$

where

$$N_1 = \sin \Theta \cos \Phi, \quad (3a)$$

$$N_2 = \sin \Theta \sin \Phi, \quad (3b)$$

$$N_3 = \cos \Theta, \quad (3c)$$

and $0 \leq \Theta \leq \pi$, $0 \leq \Phi \leq 2\pi$. Notice that, here and in the following, the notation has been changed with respect to our previous paper, for consistency with the following treatment, where second-rank Legendre polynomials $P_2(\dots)$ are to be used; we also found it advisable to use the superscript 0 for various ground-state quantities; the above configuration will be denoted by $D(\Theta, \Phi)$.

Various structural quantities can be defined, some of which are found to be zero for all values of Θ and Φ , or to average to zero upon integration over the angles; for example, when $d = 3$,

$$\sum_{j \in \Delta} \mathbf{u}_j^0 = 0, \quad (4a)$$

$$\sum_{j \in \Delta} \rho_h \mathbf{u}_j^0 = 0, \quad \sum_{j \in \Delta} \rho_k \mathbf{u}_j^0 = 0, \quad \sum_{j \in \Delta} \rho_l \mathbf{u}_j^0 = 0, \quad (4b)$$

$$\sum_{j \in \Delta} \tau_{hkl} \mathbf{u}_j^0 = 0. \quad (4c)$$

In these equations Δ denotes the d -dimensional unit cell with $\varrho = 2^d$ the number of particles in

it; other staggered magnetizations are not averaged to zero upon summing over the unit cell:

$$\mathbf{B}_1^0 = \sum_{j \in \Delta} \sigma_{kl} \mathbf{u}_j^0 = \varrho N_1 \mathbf{e}_1, \quad (5a)$$

$$\mathbf{B}_2^0 = \sum_{j \in \Delta} \sigma_{hl} \mathbf{u}_j^0 = \varrho N_2 \mathbf{e}_2, \quad (5b)$$

$$\mathbf{B}_3^0 = \sum_{j \in \Delta} \sigma_{hk} \mathbf{u}_j^0 = \varrho N_3 \mathbf{e}_3; \quad (5c)$$

thus, bearing in mind the above results, for any unit vector \mathbf{u}_j associated with the lattice site \mathbf{x}_j , one can define another unit vector \mathbf{w}_j with Cartesian components $w_{j,\kappa}$ via

$$w_{j,1} = \sigma_{kl} u_{j,1} \quad (6a)$$

$$w_{j,2} = \sigma_{hl} u_{j,2} \quad (6b)$$

$$w_{j,3} = \sigma_{hk} u_{j,3} \quad (6c)$$

and hence the staggered magnetization

$$\mathbf{C} = \sum_{j \in \Delta} \mathbf{w}_j; \quad (7)$$

when $\mathbf{u}_j = \mathbf{u}_j^0$, $j = 1, 2 \dots 8$, i.e. for the ground–state orientations (Eq. (2)), Eq. (7) leads to

$$\mathbf{C}^0 = \sum_{j \in \Delta} \mathbf{w}_j^0 = \mathbf{B}_1^0 + \mathbf{B}_2^0 + \mathbf{B}_3^0 = \varrho (N_1 \mathbf{e}_1 + N_2 \mathbf{e}_2 + N_3 \mathbf{e}_3); \quad (8)$$

in this case

$$\mathbf{w}_j^0 = N_1 \mathbf{e}_1 + N_2 \mathbf{e}_2 + N_3 \mathbf{e}_3, \quad j = 1, 2 \dots 8. \quad (9)$$

The ground–state order parameter is defined by

$$\frac{1}{\varrho} \sqrt{\mathbf{C}^0 \cdot \mathbf{C}^0} = 1. \quad (10)$$

Eqs. (3), (8) and (9) show that in all $D(\Theta, \Phi)$ configurations the vector \mathbf{C}^0 has the same modulus, and that each $D(\Theta, \Phi)$ defines its possible orientation, or, in other words, the ground state exhibits full order and continuous degeneracy with respect to the above \mathbf{C}^0 vector. Notice also that the above transformation from \mathbf{u}_j to \mathbf{w}_j unit vectors (Eq. (6)) can, and will be, used in the following for arbitrary configurations of unit vectors \mathbf{u}_j , to calculate \mathbf{C} (Eqs. (7) and (17)).

After this brief reminder about magnetic ordering, we now explore nematic ordering in the ground state. For a generic configuration $D(\Theta, \Phi)$, the nematic second-rank ordering tensor \mathbf{Q}^0 is defined by [15–17]

$$Q_{\iota\kappa}^0 = \frac{3}{2\rho} \sum_{j \in \Delta} (u_{j,\iota}^0 u_{j,\kappa}^0) - \frac{\delta_{\iota\kappa}}{2}; \quad (11)$$

the above tensor turns out to be diagonal, i.e.

$$Q_{\iota\kappa}^0 = \delta_{\iota\kappa} q_\kappa, \quad q_\kappa = P_2(N_\kappa). \quad (12)$$

The eigenvalue with the largest magnitude (to be denoted by \bar{q}) ranges between $-\frac{1}{2}$ and $+1$; some specific configurations and their corresponding \bar{q} quantities are

$$D_1 = D(0, \Phi), \quad \forall \Phi, \quad \bar{q} = +1 \quad (13a)$$

$$D_2 = D\left(\frac{\pi}{2}, \frac{\pi}{4}\right), \quad \bar{q} = -\frac{1}{2} \quad (13b)$$

$$D_3 = D\left(\arccos\left(\frac{1}{\sqrt{3}}\right), \frac{\pi}{4}\right), \quad \bar{q} = 0; \quad (13c)$$

other equivalent cases can be obtained from Eqs. (13) by appropriate choices of the two angles, corresponding to a suitable relabeling of lattice axes; for example the D_1 case can also be realized by $D\left(\frac{\pi}{2}, 0\right)$ or $D\left(\frac{\pi}{2}, \frac{\pi}{2}\right)$.

Some geometric remarks on Eq. (13) may also be appropriate. In D_1 -type configurations, all unit vectors \mathbf{u}_j^0 are oriented along a lattice axis, with appropriate signs of the corresponding components; here full nematic order is realized. In D_2 -type configurations, all unit vectors \mathbf{u}_j^0 lie on a lattice plane, and their components along the corresponding axes are $(\pm\sqrt{2}/2, \pm\sqrt{2}/2)$, with the four combinations of signs, producing antinematic order; in D_3 -type configurations, the unit vectors \mathbf{u}_j^0 have components along lattice axes given by $(\pm\sqrt{3}/3, \pm\sqrt{3}/3, \pm\sqrt{3}/3)$, with all possible combinations of signs; in the latter case, magnetic order of the unit vectors \mathbf{w}_j^0 is accompanied by no nematic order. The three named ground-state configurations are shown in FIG. 1. Notice also that, upon integrating over the two angles, the three quantities q_κ are averaged to zero; in other words, *the ground-state possesses ferromagnetic order with respect to the \mathbf{C}^0 -vector, but its degeneracy destroys overall nematic order.* On the other hand, models with simple ferromagnetic or antiferromagnetic interactions (say nearest-neighbour interactions isotropic in spin space and on a bipartite lattice) also produce a secondary nematic (even-rank) order, in addition to the first-rank one [12–14]. One could, for example, compare the present case with a classical Heisenberg model, on a simple-cubic lattice, and with isotropic ferromagnetic interactions restricted to nearest neighbours: in this latter case, each possible orientation of the magnetic ordering vector corresponds

to full nematic order. Let us also mention that there exist models involving discrete site variables and competing magnetic interactions at different scales, and which can produce striped or “Ising nematic” order, but no simple magnetic one; see, e.g., Ref. [18] and others quoted therein.

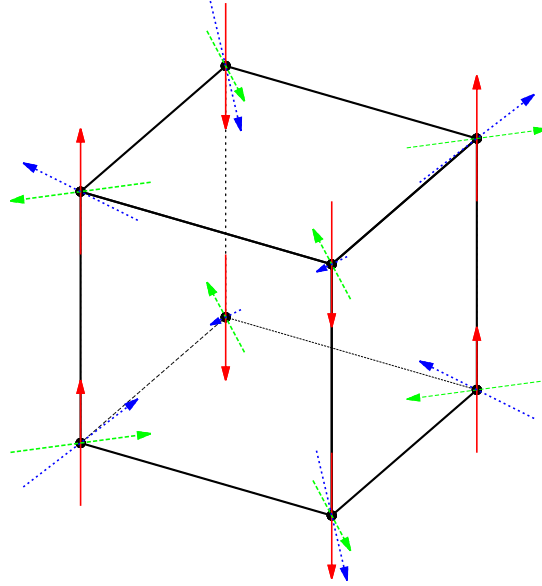


FIG. 1: (Color on line) The present figure shows the cubic unit cell for the model under investigation, together with the three ground–state configurations discussed in the text (Eq. (13)), with spin orientations represented by appropriate arrows. Meaning of symbols: (red) continuous line: D_1 configuration; (green) dashed line: D_2 configuration; (blue) dotted line: D_3 configuration; black lines mark cell edges, and black dots identify the vertices.

What happens at suitably low but finite temperatures? Overall magnetic order (in terms of \mathbf{C} vector) survives (recall also the mathematical result [9]); on the other hand, different D configurations might be affected by fluctuations to different extents, possibly to the extreme situation where only some of them are thermally selected (“survive”); this behavior, studied in a few cases after 1980, is known as ordering by disorder, see, e.g. Refs. [19–25]. For some interaction models, involving 2–component spins on a 2–dimensional lattice, such a result was mathematically proven [25]; in other cases (also involving 2–component spins and 2–dimensional lattices) the result was obtained by an approximate harmonic (spin–wave) treatment [20, 21]. In other cases, involving 3–dimensional lattices, the onset of ordering by disorder at suitably low but finite temperature is borne out by simulation [23, 24]; notice also that the prediction in Ref. [21] was not confirmed by subsequent simulations in Ref. [22].

Actually, our additional simulations, presented in Section IV, showed evidence of nematic order by disorder: it was observed that simulations started at low temperature from different configurations $D(\Theta, \Phi)$ quickly resulted in configurations remaining close to the above D_1 type, i.e. the \mathbf{C} -vector remained aligned with a lattice axis; this caused the onset of second-rank nematic order, as shown by sizable values of the corresponding order parameters \bar{P}_2 and \bar{P}_4 (see following Sections); in turn, the nematic director remained aligned with the above \mathbf{C} -vector (this aspect is further treated by Eq. (24) and then FIG. (9)).

III. COMPUTATIONAL ASPECTS AND FINITE-SIZE SCALING THEORY

Calculations were carried out using periodic boundary conditions, and on samples consisting of $N = L^3$ particles, with $L = 10, 12, 16, 20, 24, 32$. Simulations, based on standard Metropolis updating algorithm, were carried out in cascade, in order of increasing temperature T ; equilibration runs took between 25000 and 50000 cycles (where one cycle corresponds to $2N$ attempted Monte Carlo steps, including sublattice sweeps (checkerboard decomposition [26–29]), and production runs took between 500000 and 1000000; each attempted Monte Carlo step also included overrelaxation [30–34].

As for the cycle length used here, let us first notice that the parity of each lattice site k can be defined via the sum of its coordinates; a lattice \mathbb{Z}^d is geometrically bipartite, i.e it consists of two interpenetrating sublattices of even and odd parities, respectively; moreover, the potential is restricted to nearest neighbours, hence there is no interaction between spins associated with lattice sites of the same parity, and the outcomes of Monte Carlo attempts taking place at different sites of the same parity are independent of one another. Each sweep (or cycle) used here consisted of $2N$ attempts, first N attempts where the lattice site was chosen randomly, then $N/2$ sequential attempts on lattice sites of odd parity, and finally $N/2$ sequential attempts on lattice sites on even parity. Subaverages for evaluating statistical errors were calculated over macrosteps consisting of 1000 cycles.

Calculated quantities include the potential energy in units ϵ per particle,

$$U = \frac{\langle W \rangle}{N}, \quad (14)$$

where

$$W = \frac{1}{2\epsilon} \sum_{i \neq j} V_{ij} \quad (15)$$

is the total potential energy of the system, and configurational specific heat

$$\frac{C_V}{k_B} = \frac{1}{NT^2} (\langle W^2 \rangle - \langle W \rangle^2), \quad (16)$$

where $\langle \dots \rangle$ denotes statistical averages. Mean staggered magnetization and corresponding susceptibility [35, 36] are defined via the appropriate generalizations of Eqs. (6) and (7), now involving all the spins in the sample, and by the formulae:

$$M = \frac{1}{N} \langle |\mathbf{C}| \rangle, \quad M_2 = \frac{1}{N} \langle \mathbf{C} \cdot \mathbf{C} \rangle, \quad \mathbf{C} = \sum_{j=1}^N \mathbf{w}_j \quad (17)$$

$$\chi = \begin{cases} \frac{1}{T} (M_2 - NM^2), & T < T_c \\ \frac{1}{T} M_2, & T \geq T_c \end{cases}; \quad (18)$$

analysis of simulation results for the three Cartesian components of \mathbf{C} showed that, in the ordered region, the named vector remained close to a lattice axis.

We also calculated both second- and fourth-rank nematic order parameters [15–17], by analyzing one configuration every cycle; more explicitly, for a generic examined configuration, the \mathbf{Q} tensor is defined by the appropriate generalization of Eq. (11), now involving all the spins in the sample; in formulae

$$Q_{i\kappa} = \frac{1}{2} (3F_{i\kappa} - \delta_{i\kappa}), \quad (19)$$

with

$$F_{i\kappa} = \langle u_i u_\kappa \rangle_{loc} = \frac{1}{N} \sum_{j=1}^N (u_{j,i} u_{j,\kappa}), \quad (20)$$

where $\langle \dots \rangle_{loc}$ denotes average over the current configuration; the fourth-rank order parameter comes from the analogous quantity [37]

$$\begin{aligned} B_{i\kappa\lambda\mu} = & \frac{1}{8} [35G_{i\kappa\lambda\mu} - 5(\delta_{i\kappa}F_{\lambda\mu} + \delta_{i\lambda}F_{\kappa\mu} + \delta_{i\mu}F_{\kappa\lambda} \\ & + \delta_{\kappa\lambda}F_{i\mu} + \delta_{\kappa\lambda}F_{i\mu} + \delta_{\lambda\mu}F_{i\kappa}) \\ & + (\delta_{i\kappa}\delta_{\lambda\mu} + \delta_{i\lambda}\delta_{\kappa\mu} + \delta_{i\mu}\delta_{\kappa\lambda})], \end{aligned} \quad (21)$$

where

$$G_{i\kappa\lambda\mu} = \langle u_i u_\kappa u_\lambda u_\mu \rangle_{loc} = \frac{1}{N} \sum_{j=1}^N u_{j,i} u_{j,\kappa} u_{j,\lambda} u_{j,\mu}. \quad (22)$$

The calculated tensor \mathbf{Q} was diagonalized; let ω_k denote its three eigenvalues, and let \mathbf{v}_k denote the corresponding eigenvectors; the eigenvalue with the largest magnitude (usually a positive number, thus the maximum eigenvalue), can be identified, and its average over the simulation chain defines the nematic second-rank order parameter \overline{P}_2 ; the corresponding eigenvector defines the local (fluctuating) configuration director \mathbf{n} [15–17], evolving along the simulation. Actually, a suitable reordering of eigenvalues (and hence of the corresponding eigenvectors) is needed for evaluating \overline{P}_4 ; let the eigenvalues ω_k be reordered (i.e. permuted, according to some rule), to yield the values ω'_k ; the procedure used here as well as in other previous papers (e.g. Refs. [38, 39]) involves a permutation such that

$$|\omega'_3| \geq |\omega'_1|, |\omega'_3| \geq |\omega'_2|; \quad (23a)$$

actually there exist two such possible permutations, an odd and an even one; we consistently chose permutations of the same parity (say even ones, see also below) for all examined configurations; recall that eigenvalue reordering also induces the corresponding permutation of the associated eigenvectors. Notice also that, in most cases, $\omega'_3 > 0$, so that the condition in Eq. (23a) reduces to

$$\omega'_3 \geq \omega'_1, \omega'_3 \geq \omega'_2; \quad (23b)$$

this latter procedure was considered in earlier treatments of the method. As already mentioned, the second-rank order parameter \overline{P}_2 is defined by the average of ω'_3 over the simulation chain; on the other hand, the quantity $(\omega'_2 - \omega'_1)$, and hence its average over the chain, measure possible phase biaxiality, found here to be zero within statistical errors, as it should. The procedure outlined here was previously used elsewhere [38–43], in cases where some amount of biaxial order might exist; the consistent choice of permutations of the same parity was found to avoid both artificially enforcing a spurious phase biaxiality (as would result by imposing an additional condition such as $|\omega'_1| \leq |\omega'_2|$), and artificially reducing or even quenching it (as would result by ordering ω'_1 and ω'_2 at random).

The fourth-rank order parameter was evaluated from the \mathbf{B} tensor in the following way [37]: for each analyzed configuration, the suitably reordered eigenvectors of \mathbf{Q} define the director frame, and build the column vectors of an orthogonal matrix \mathbf{R} , in turn employed for transforming \mathbf{B} to the director frame; the diagonal element B'_{3333} of the transformed tensor was averaged over the production run, and identified with \overline{P}_4 .

Moreover, an indicator of the correlation between staggered magnetization and even-rank orientational order could be worked out. For a given configuration, let \mathbf{n} denote the nematic director,

and let \mathbf{m} be the unit vector defined by \mathbf{C} ; thus we calculated

$$\phi = \langle |\mathbf{m} \cdot \mathbf{n}| \rangle. \quad (24)$$

Notice that, by rotational invariance, one of the two unit vectors can be taken to define the z -axis; upon expressing the orientation of the other unit vector in terms of usual polar and azimuthal angles Θ and Φ , one obtains

$$\phi = \langle |\cos \Theta| \rangle, \quad (25)$$

so that ϕ ranges between $\frac{1}{2}$ for random mutual orientation of the two unit vectors, and 1 when they are strictly parallel or antiparallel.

To gain insights into the critical behaviour of the model under consideration, we analyse the simulation results according to Finite-Size Scaling (FSS) theory [26, 44]. This theory states that the bulk critical behaviour is altered by finite-size effects when the system is subjected to boundaries (the interested reader is invited to consult Ref. [45], containing also numerous relevant references). For systems confined to a cubic box with volume L^3 under periodic boundary conditions, any *size*-dependent thermodynamic quantity $O(L, T)$, that behaves in the bulk limit as $O(\infty, T) \sim t^{-\nu}$ (with $t = \left(1 - \frac{T}{T_c}\right) \ll 1$, being the deviation from the bulk critical point T_c), is expected to scale like

$$O(L, T) = L^{\nu/\nu} \Xi_O(tL^{1/\nu}), \quad (26)$$

where ν is the critical exponent measuring the divergence of the correlation length ξ as we approach the critical point i.e. $\xi \sim t^{-\nu}$ and $\Xi_O(x)$ is a scaling function up to a multiplicative non universal quantity. Furthermore, the singularities taking place in the bulk system are rounded, with maxima, corresponding to a shifted temperature located at a distance, proportional to $L^{-1/\nu}$, from the critical temperature. Notice that the scaling form (26) holds only asymptotically close to the critical point i.e. it is valid for sizes $L \gg 1$ and $\xi \gg 1$. In this limit corrections to FSS do not affect the *universal* finite-size behaviour i.e. quantities that are independent of the microscopic details of the system.

The scaling behaviour (26) suggests that simulation data for the different system sizes should fall onto the same curve for a suitable choice of a set of critical exponents and critical temperature, thus allowing to estimate their values using a data collapse procedure. For the purposes of this paper we have used the algorithm of Ref. [46], which is based on the minimization approach of

Ref. [47] to fit data for the different sample sizes. The quality of data collapse is measured by a fitting-parameter dependent function S whose value should be approximately 1.

An important quantity for any FSS analysis is the fourth-order cumulant, also known as the Binder cumulant [48]

$$U_L = 1 - \frac{\langle(\mathbf{C} \cdot \mathbf{C})^2\rangle}{3\langle\mathbf{C} \cdot \mathbf{C}\rangle^2}. \quad (27)$$

It obeys the scaling law (26) with $\varkappa = 0$ [26, 44]. Thus its value at the bulk critical point is independent of the linear size of the system. This property provides the best tool to locate the critical point as the intersection of the plots of U_L for different sample sizes L against the temperature. For the model considered here, U_L varies between $\frac{2}{3}$ at $T = 0$ i.e when the spins point in the same orientation (ordered phase) and $\frac{4}{9}$ at $T \rightarrow \infty$ with spins randomly oriented in space (disordered phase). In the Appendix we present our computational details relevant to the high temperature limit for arbitrary number n of spin components, including Ising and plane rotator models, as well as the corresponding result for the xy model, for the sake of completeness.

IV. RESULTS

Simulations estimates of the potential energy per spin (not shown here) were found to vary in a gradual and continuous fashion against temperature and seemed to be largely unaffected by sample size to within statistical errors ranging up to 0.5%. In addition, they exhibited a smooth change of slope at about $T \approx 1.86$. This change is reflected on the behaviour of the specific heat, whose fluctuation results showed a recognizably size dependent maximum around the same temperature – the height of the maximum increases and the “full width at half maximum” decreases as the system size increases (FIG. 2); this behaviour seems to develop into a singularity in the infinite-sample limit.

Results for the mean staggered magnetization M , plotted in FIG. 3, were found to decrease with temperature at fixed sample size. For temperatures below 1.8 the data for different sample sizes practically coincide, while for larger temperatures the magnetization decreases significantly as the system size increases. The fluctuations of M versus temperature are investigated through the susceptibility χ , shown in FIG. 4. We observed a pronounced growth of this quantity with the system size at about $T = 1.89$. This is manifested by a significant increase in the maximum height, as well as a shrinking of the “full width at half maximum”, suggesting that the susceptibility will show a singularity as the system size goes to infinity. This behaviour is an evidence of the onset

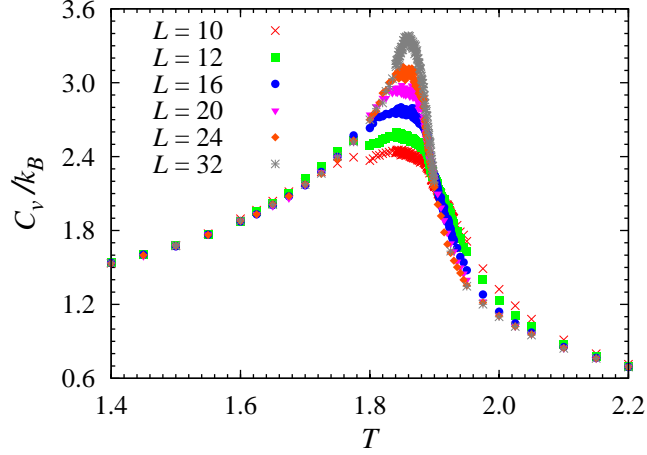


FIG. 2: Simulation results for the configurational specific heat, obtained with different sample sizes; the statistical errors (not shown) range between 1 and 5%.

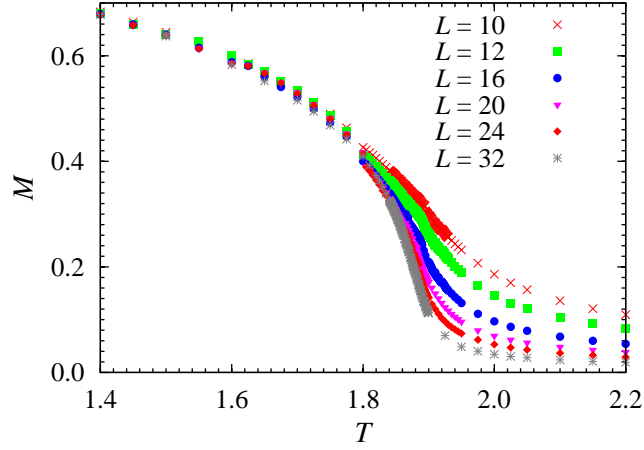


FIG. 3: Simulation estimates for the mean staggered magnetization M , obtained with different sample sizes; here and in the following figures, the errors fall within symbol size.

of a second order phase transition.

Let us now turn our attention to the FSS analysis of the simulation results. According to FSS theory the magnetization scales like

$$M = L^{-\beta/\nu} \Xi_M(tL^{1/\nu}), \quad (28)$$

showing that the magnetization behaves as $L^{-\beta/\nu}$ at $T = T_c$ for finite systems. Analysing the simulation data of FIG. 3 we obtain the behavior of the scaling function $\Xi_M(x)$. This is depicted in FIG. 5. Fitting the data for different sample sizes to the scaling form (28), and excluding

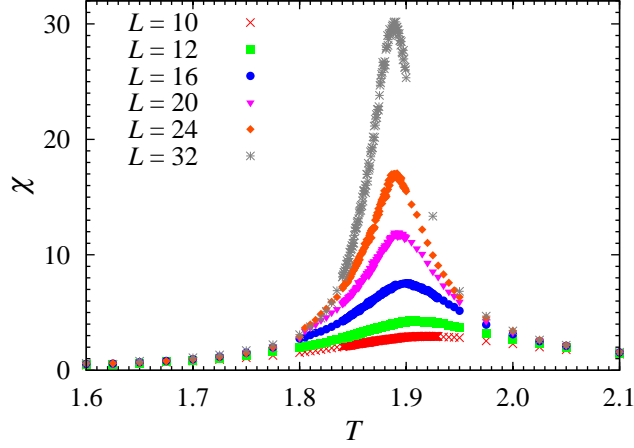


FIG. 4: Simulation estimates for the susceptibility χ associated with the staggered magnetization M , obtained with different sample sizes.

smaller sizes subsequently, we get the results presented in Table I. Our best estimate is obtained for $S = 1.1888$ corresponding to the critical temperature $T_c = 1.8806 \pm 0.0002$ and critical exponents $\nu = 0.713 \pm 0.001$ and $\beta = 0.358 \pm 0.006$.

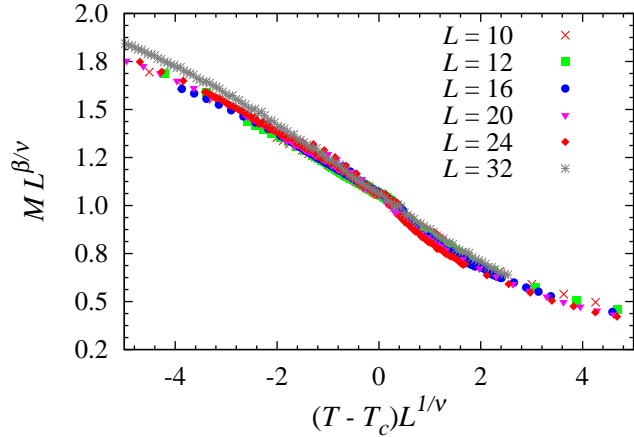


FIG. 5: Scaling behaviour of the magnetization M .

A similar analysis is performed on the simulation data for the susceptibility whose scaling form is given by

$$\chi = L^{\gamma/\nu} \Xi_{\chi}(tL^{1/\nu}). \quad (29)$$

FSS analysis of the corresponding data yields the results summarized in Table II. Notice that the best data collapse is obtained for $16 \leq L \leq 32$ with $S = 1.2971$ and the set of critical values: $T_c = 1.877 \pm 0.001$, $\nu = 0.71 \pm 0.04$ and $\gamma = 1.4 \pm 0.1$. In turn, the scaling law for the specific

TABLE I: Outcome from data collapse of the staggered magnetization obtained with different sample sizes.

$L_{\min} - L_{\max}$	T_c	$\frac{1}{\nu}$	$\frac{\beta}{\nu}$	S
10 – 32	1.8787 ± 0.0002	1.415 ± 0.008	0.483 ± 0.003	6.8341
12 – 32	1.8798 ± 0.0005	1.409 ± 0.002	0.496 ± 0.003	13.335
16 – 32	1.8806 ± 0.0002	1.403 ± 0.001	0.503 ± 0.006	0.8795
20 – 32	1.8801 ± 0.0001	1.40 ± 0.01	0.502 ± 0.009	1.1888

heat

$$C_v = L^{\alpha/\nu} \Xi_C (tL^{1/\nu}) \quad (30)$$

leads to $S = 1.0877$ and the critical estimates $T_c = 1.8802 \pm 0.0004$, $\nu = 0.71 \pm 0.02$ and $\alpha = 0.13 \pm 0.02$. All these results are clear evidence that the considered model belongs to the Heisenberg universality class with a critical temperature $T_c = 1.877 \pm 0.001$. Let us point out that in general the results obtained for the critical exponents are consistent with their corresponding values in Ref. [10], whereas that of the transition temperature has been refined. This is due to the fact that we used larger sample sizes compared to those analyzed there.

TABLE II: Same as Table I for the magnetic susceptibility

$L_{\min} - L_{\max}$	T_c	$\frac{1}{\nu}$	$\frac{\gamma}{\nu}$	S
10 – 32	1.877 ± 0.001	1.40 ± 0.10	-1.97 ± 0.02	1.2409
12 – 32	1.877 ± 0.001	1.40 ± 0.10	-1.97 ± 0.02	1.2888
16 – 32	1.877 ± 0.001	1.40 ± 0.10	-1.96 ± 0.03	1.2971
20 – 32	1.878 ± 0.003	1.40 ± 0.08	-1.96 ± 0.05	1.3158

TABLE III: Same as Table I for the configurational specific heat

$L_{\min} - L_{\max}$	T_c	$\frac{1}{\nu}$	$\frac{\alpha}{\nu}$	S
10 – 32	1.8839 ± 0.0009	1.40 ± 0.03	-0.187 ± 0.004	18.8678
12 – 32	1.883 ± 0.002	1.39 ± 0.05	-0.184 ± 0.006	12.5743
16 – 32	1.8802 ± 0.0004	1.40 ± 0.06	-0.18 ± 0.01	1.0877
20 – 32	1.8791 ± 0.0006	1.40 ± 0.04	-0.18 ± 0.01	1.9356

Simulation estimates for the fourth-order cumulant U_L obtained for different sample sizes as a function of temperature are shown on FIG. 6. The plots for the different curves are found to decrease against the temperature and to intersect at $T_c = 1.8795 \pm 0.0005$. The corresponding critical amplitude is $U_L^* \approx 0.617$. At the two extremes of zero temperature and that of infinite temperature U_L has exactly the theoretically predicted values that are size independent.

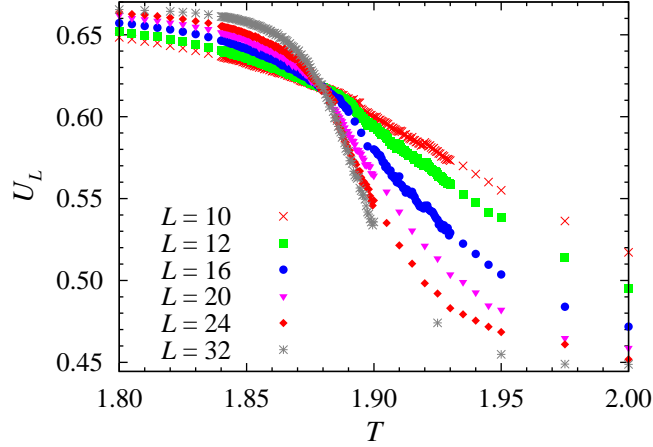


FIG. 6: Simulation results for the fourth-order cumulant (27) obtained with different sample sizes.

Simulation results for the nematic order parameter \overline{P}_2 are plotted in FIG. 7; they show a gradual and monotonic decrease with temperature, vanishing above T_c , and appear to be mildly affected by sample sizes; simulation results for \overline{P}_4 (see FIG. 8) exhibited a qualitatively similar behaviour; in the low-temperature region, say $T \leq 0.25$ (figures not shown), simulation results for these two quantities appear to saturate to 1 as $T \rightarrow 0$. According to FSS approach the nematic order parameter is expected to scale as

$$\overline{P}_2 = L^{-2\beta/\nu} \Xi(tL^{1/\nu}). \quad (31)$$

Applying the above mentioned minimization procedure we get $T_c = 1.8796 \pm 0.0009$, $\frac{2\beta}{\nu} = 1.02 \pm 0.03$ and $\frac{1}{\nu} = 1.39 \pm 0.06$ in a very good agreement with the above finding for the staggered magnetization.

Simulation data for ϕ (Eq. (24)) are plotted in FIG. 9 for all investigated sample sizes they appear to decrease with increasing temperature; moreover, the results exhibit a recognizable increase of ϕ with increasing sample size for $T \lesssim T_1 = 1.88$, and its recognizable decrease with increasing sample size for $T \gtrsim T_2 = 1.89$, so that the seemingly continuous change across the transition region becomes steeper and steeper as sample size increases. In the crossover temperature range

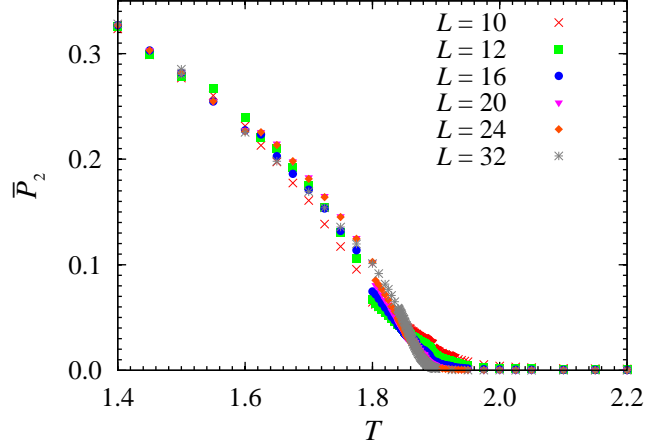


FIG. 7: Simulation results for the nematic second-rank order parameter \overline{P}_2 , obtained with different sample sizes.

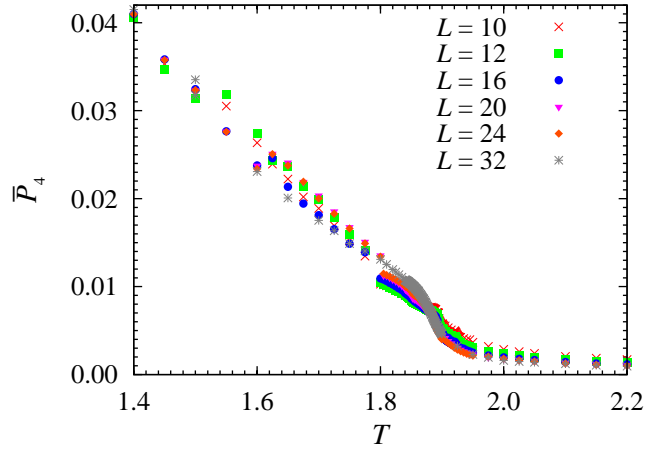


FIG. 8: Simulation results for the nematic second-rank order parameter \overline{P}_4 , obtained with different sample sizes.

between T_1 and T_2 the sample-size dependence of results becomes rather weak, and the various curves come close to coincidence at $T \approx 1.8830 \pm 0.0005$, with $\phi \approx 0.666 \approx \frac{2}{3}$; notice that this temperature value is in reasonable agreement with T_c as independently estimated via the above FSS treatment.

V. CONCLUSIONS

We have studied the transitional behaviour of the lattice-spin model in Ref. [10], by means of larger-scale simulation as well as a detailed analysis of results; FSS basically confirms the

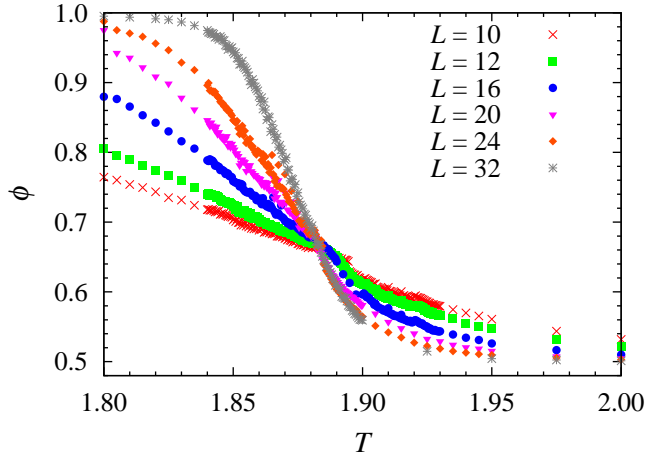


FIG. 9: Simulation results for the quantity ϕ , as defined in the text (Eq. 24), obtained with different sample sizes.

Heisenberg universality class with a critical temperature $T_c = 1.877 \pm 0.001$; analysis of second-rank properties has shown the existence of secondary nematic order, destroyed by ground state degeneracy but restored the low-temperature phase, through a mechanism of order by disorder [19–25]. In experimental terms, the nematic–isotropic transition for single-component systems is known to be weakly first-order, whereas here the overall ordering transition is second-order

By now, both polar and apolar mesogens (e.g. para-quinque-phenyl) are known experimentally, and various theoretical treatments have been developed based on interactions of even symmetry (say Onsager theory for hard spherocylinders, or the Molecular Field approach by Maier and Saupe); interaction models of even symmetry have been studied by simulation, e.g. the Lebwohl–Lasher model, or the Gay–Berne model(s) with different sets of parameters [49]; hard-core and Gay–Berne models supplemented by dipolar or quadrupolar terms have been discussed as well [49]; this body of evidence shows that dipolar interactions are not essential for nematic behaviour, but they can significantly modulate it. As mentioned in the Introduction, dipolar hard spheres are predicted to produce a polar (ferroelectric) nematic phase [8]; experimental realizations of such fluid phases consisting of low molecular mass thermotropic mesogens have been actively looked for, but, to the best of our knowledge, not found so far (see, e.g. Ref. [50] and others quoted therein).

Acknowledgements

The present extensive calculations were carried out, on, among other machines, workstations, belonging to the Sezione di Pavia of Istituto Nazionale di Fisica Nucleare (INFN); allocations of computer time by the Computer Centre of Pavia University and CILEA (Consorzio Interuniversitario Lombardo per l'Elaborazione Automatica, Segrate - Milan), as well as by CINECA (Centro Interuniversitario Nord-Est di Calcolo Automatico, Casalecchio di Reno - Bologna), and CASPUR (Consorzio interuniversitario per le Applicazioni di Supercalcolo per Università e Ricerca, Rome) are gratefully acknowledged.

Appendix: Binder Cumulant at high temperatures

Let $N = L^3$ denote the total number of elements in a set of n -component random unit vectors $\{\mathbf{g}_j, j = 1, 2, \dots, N\}$, coupled by some general odd interaction where all their n components are involved, and let

$$\mathbf{P} = \sum_{j=1}^N \mathbf{g}_j, \quad (\text{A.1})$$

be the sum of all vectors in the set. Introducing the notations

$$S_2 = \mathbf{P} \cdot \mathbf{P} = \sum_{j=1}^N \sum_{k=1}^N \mathbf{g}_j \cdot \mathbf{g}_k, \quad (\text{A.2a})$$

$$S_4 = S_2 \cdot S_2 = \sum_{j=1}^N \sum_{k=1}^N \sum_{p=1}^N \sum_{q=1}^N (\mathbf{g}_j \cdot \mathbf{g}_k) (\mathbf{g}_p \cdot \mathbf{g}_q), \quad (\text{A.2b})$$

we define the moments related to \mathbf{P} by

$$s_2 = \langle S_2 \rangle_f, \quad (\text{A.3a})$$

$$s_4 = \langle S_4 \rangle_f, \quad (\text{A.3b})$$

where the subscript f means averaging with respect to orientations of all the unit vectors, to be treated as independent variables, with usual rotation-invariant probability measures; in other words, the subscript f means completely neglecting interactions. In physical terms, $\langle \dots \rangle_f$ means averaging at infinite temperature; in simulation the limit is approached at sufficiently high temperature, in the orientationally disordered region, see FIG. 6.

After some algebra one obtains

$$\langle \mathbf{g}_j \cdot \mathbf{g}_k \rangle_f = \delta_{jk}, \quad (\text{A.4a})$$

where δ_{jk} is the Kronecker symbol, and

$$\langle (\mathbf{g}_j \cdot \mathbf{g}_k) (\mathbf{g}_p \cdot \mathbf{g}_q) \rangle_f = 0, \quad (\text{A.4b})$$

when the expression contains at least three different subscripts, or when it contains odd powers of scalar products between different unit vectors; on the other hand

$$\langle (\mathbf{g}_j \cdot \mathbf{g}_k)^2 \rangle_f = \delta_{jk} + \frac{1 - \delta_{jk}}{n}. \quad (\text{A.4c})$$

Actually this result holds for all $n > 1$ and by the underlying $O(n)$ rotational invariance, it can be obtained with the aid of

$$\langle \cos^2 \theta \rangle = \frac{\int_0^\pi \cos^2 \theta \sin^{n-2} \theta d\theta}{\int_0^\pi \sin^{n-2} \theta d\theta} = \frac{1}{n}, \quad n > 1. \quad (\text{A.5})$$

This is a direct consequence of the fact that in hyperspherical coordinates one integrates over the solid angle

$$d^n S = \sin^{n-2} \theta \sin^{n-3} \varphi_1 \sin^{n-4} \varphi_2 \cdots \sin \varphi_{n-3} d\theta d\varphi_1 \cdots d\varphi_{n-3} d\varphi_{n-2}, \quad (\text{A.6})$$

with $0 \leq \theta \leq \pi$, $0 \leq \varphi_1 \leq \pi$, \dots , $0 \leq \varphi_{n-2} \leq 2\pi$, and integrations over all angles but θ in the measure cancel out; notice that Eq. (A.5) also holds for $n = 2$ (plane rotators), where only one angle is involved, ranging between 0 and 2π .

Substituting Eqs. (A.4) into Eqs. (A.3) we obtain

$$s_2 = N, \quad (\text{A.7a})$$

$$s_4 = N^2 + \frac{2}{n}N(N-1), \quad (\text{A.7b})$$

so that the fourth-order cumulant is essentially defined by

$$\frac{s_4}{(s_2)^2} = 1 + \frac{2}{n} - \frac{2}{nN}; \quad (\text{A.7c})$$

notice that the results also hold for $n = 1$ (Ising spins). Setting $n = 3$ and taking the limit $N \rightarrow \infty$ in (A.7c) we get our result mentioned in the text.

Notice that the previous results hold in a rather wide setting, e. g. for rather general odd interactions among the spins (actually these formulae are obtained in the limit of no interactions); thus they can be specialized to the case discussed in the main text, possibly by substituting \mathbf{g}_j with \mathbf{w}_j and \mathbf{P} with \mathbf{C} , for notational consistency.

In the above examples, all n spin components are assumed to be involved in the interaction, and are equally represented in the definition of the ordering quantity \mathbf{P} ; on the other hand, the xy model involves three-component spins (parameterized by usual polar angles θ_j , ϕ_j , but only two components are explicitly coupled by the interaction. In this case the above analysis has to be suitably modified, starting from

$$\mathbf{P} = \sum_{j=1}^N (g_{j,1}\mathbf{e}_1 + g_{j,2}\mathbf{e}_2), \quad (\text{A.8})$$

and substituting the above scalar products with

$$E_{jk} = \sin(\theta_j) \sin(\theta_k) \cos(\phi_j - \phi_k), \quad (\text{A.9})$$

so that

$$S_2 = \sum_{j=1}^N \sum_{k=1}^N E_{jk}, \quad (\text{A.10a})$$

$$S_4 = \sum_{j=1}^N \sum_{k=1}^N \sum_{p=1}^N \sum_{q=1}^N (E_{jk} E_{pq}). \quad (\text{A.10b})$$

As in the previous case, various terms drop by symmetry, i.e.

$$\langle E_{jk} \rangle_f = \frac{2}{3} \delta_{jk}, \quad (\text{A.11a})$$

and

$$\langle E_{jk} E_{pq} \rangle_f = 0, \quad (\text{A.11b})$$

when the expression contains at least three different subscripts, or when it contains odd powers of E terms; on the other hand

$$\langle E_{jk}^2 \rangle_f = \frac{8}{15} \delta_{jk} + 2 \frac{1 - \delta_{jk}}{9}. \quad (\text{A.11c})$$

Thus

$$s_2 = \frac{2}{3} N \quad (\text{A.12a})$$

$$s_4 = \frac{8}{15} N^2 + \frac{4}{9} N(N-1) \quad (\text{A.12b})$$

so that, in this case, the fourth-order cumulant is essentially defined by

$$\frac{s_4}{(s_2)^2} = \frac{6}{5} + \frac{N-1}{N}. \quad (\text{A.12c})$$

Here the interaction among spins has been assumed to be odd; on the other hand, when the interaction is taken to be even, one obtains the trivial result $\langle S_2 \rangle = s_2$ at all temperatures, and a different order parameter must be worked out; actually, the above definitions can be applied for interactions with a non-zero odd part.

-
- [1] D. E. Stogryn and A. P. Stogryn, [Mol. Phys. **11**, 371 \(1966\)](#).
 - [2] C. G. Gray and K. E. Gubbins, *Theory of molecular fields*, International Series of Monographs on Chemistry, Vol. 1 (Clarendon Press, Oxford, 1984).
 - [3] A. J. Stone, *The theory of intermolecular forces*, 2nd ed. (Oxford University Press, Oxford, 2013).
 - [4] A. L. Hickey and C. N. Rowley, [J. Phys. Chem. A **118**, 3678 \(2014\)](#).
 - [5] M. P. Allen and D. J. Tildesley, *Computer Simulation of Liquids* (Oxford University Press, 1989).
 - [6] S. Cardamone, T. J. Hughes, and P. L. A. Popelier, [Phys. Chem. Chem. Phys. **16**, 10367 \(2014\)](#).
 - [7] E. G. Virga, [J. Phys.: Condens. Matter **25**, 465109 \(2013\)](#).
 - [8] D. Levesque and J.-J. Weis, [J. Chem. Phys. **140**, 094507 \(2014\)](#).
 - [9] J. Fröhlich and T. Spencer, [J. Stat. Phys. **24**, 617 \(1981\)](#).
 - [10] S. Romano, [Phys. Rev. B **49**, 12287 \(1994\)](#).
 - [11] A. Giuliani, [J. Stat. Phys. **134**, 1059 \(2009\)](#).
 - [12] S. Romano and R. O. Sokolovskii, [Phys. Rev. B **61**, 11379 \(2000\)](#).
 - [13] H. Chamati and S. Romano, [Phys. Rev. B **72**, 064424 \(2005\)](#).
 - [14] H. Chamati and S. Romano, [Phys. Rev. B **72**, 064444 \(2005\)](#).
 - [15] C. Zannoni, in *The molecular physics of liquid crystals*, edited by G. R. Luckhurst and G. W. Gray (Academic Press, London, 1979) Chap. 3, p. 51.
 - [16] C. Zannoni, in *The molecular physics of liquid crystals*, edited by G. R. Luckhurst and G. W. Gray (Academic Press, London, 1979) Chap. 9, p. 191.
 - [17] C. Zannoni, in *Advances in the Computer Simulations of Liquid Crystals*, NATO Science Series No. 545, edited by P. Pasini and C. Zannoni (Springer, Dordrecht, 2000) p. 17.
 - [18] D. G. Barci, L. Ribeiro, and D. A. Stariolo, [Phys. Rev. E **87**, 062119 \(2013\)](#).
 - [19] J. Villain, R. Bidaux, J.-P. Carton, and R. Conte, [J. Physique **41**, 1263 \(1980\)](#).
 - [20] C. L. Henley, [Phys. Rev. Lett. **62**, 2056 \(1989\)](#).
 - [21] S. Prakash and C. L. Henley, [Phys. Rev. B **42**, 6574 \(1990\)](#).

- [22] S. Romano, *Phys. Scr.* **50**, 326 (1994).
- [23] C. Yamaguchi and Y. Okabe, *J. Phys. A: Math. Gen.* **34**, 8781 (2001).
- [24] S. Romano and G. De Matteis, *Phys. Rev. E* **84**, 011703 (2011).
- [25] M. Biskup, L. Chayes, and S. A. Kivelson, *Ann. Henri Poincaré* **5**, 1181 (2004).
- [26] K. Binder and D. W. Heermann, *Monte Carlo Simulation in Statistical Physics: An Introduction*, 5th ed., Graduate Texts in Physics (Springer, 2010).
- [27] C. W. Greeff and M. A. Lee, *Phys. Rev. E* **49**, 3225 (1994).
- [28] S. Romano, *Int. J. Mod. Phys. B* **9**, 85 (1995).
- [29] R. Hashim and S. Romano, *Int. J. Mod. Phys. B* **13**, 3879 (1999).
- [30] J. F. Fernández and T. S. J. Streit, *Phys. Rev. B* **25**, 6910 (1982).
- [31] R. Gupta, J. DeLapp, G. G. Batrouni, G. C. Fox, C. F. Baillie, and J. Apostolakis, *Phys. Rev. Lett.* **61**, 1996 (1988).
- [32] Y.-H. Li and S. Teitel, *Phys. Rev. B* **40**, 9122 (1989).
- [33] R. Gupta and C. F. Baillie, *Phys. Rev. B* **45**, 2883 (1992).
- [34] Y. Kadana and J. Mori, *Phys. Lett. A* **190**, 323 (1994).
- [35] T. T. A. Paauw, A. Compagner, and D. Bedeaux, *Physica A* **79**, 1 (1975).
- [36] P. Peczak, A. M. Ferrenberg, and D. P. Landau, *Phys. Rev. B* **43**, 6087 (1991).
- [37] C. Chiccoli, P. Pasini, F. Biscarini, and C. Zannoni, *Mol. Phys.* **65**, 1505 (1988).
- [38] R. Hashim, G. R. Luckhurst, F. Prata, and S. Romano, *Liq. Cryst.* **15**, 283 (1993).
- [39] S. Romano, *Int. J. Mod. Phys. B* **8**, 3389 (1994).
- [40] S. Romano, *Phys. Lett. A* **302**, 203 (2002).
- [41] S. Romano, *Phys. Lett. A* **305**, 196 (2002).
- [42] S. Romano, *Physica A* **322**, 432 (2003).
- [43] S. Romano, *Phys. Lett. A* **310**, 465 (2003).
- [44] M. E. J. Newman and G. T. Barkema, *Monte Carlo Methods in Statistical Physics* (Oxford University Press, New York, 1999).
- [45] H. Chamati, in *Advances in Planar Lipid Bilayers and Liposomes*, Vol. 17, edited by A. Iglič and J. Genova (Academic Press, 2013) p. 237.
- [46] O. Melchert, “autoScale.py - a program for automatic finite-size scaling analyses: A user’s guide,” (2009), [arXiv:0910.5403](https://arxiv.org/abs/0910.5403) [physics.comp-ph] .
- [47] J. Houdayer and A. Hartmann, *Phys. Rev. B* **70**, 014418 (2004).

- [48] K. Binder, *Z. Phys. B* **43**, 119 (1981).
- [49] M. A. Bates and G. R. Luckhurst, in *Liquid Crystals I*, Structure and Bonding No. 94, edited by D. M. P. Mingos (Springer Berlin Heidelberg, 1999) p. 65.
- [50] O. Francescangeli, V. Stanic, S. I. Torgova, A. Strigazzi, N. Scaramuzza, C. Ferrero, I. P. Dolbnya, T. M. Weiss, R. Berardi, L. Muccioli, S. Orlandi, and C. Zannoni, *Adv. Funct. Mater.* **19**, 2592 (2009).